Journal of Applied Geophysics 108 (2014) 194–198

Contents lists available at ScienceDirect

Journal of Applied Geophysics

journal homepage: www.elsevier.com/locate/jappgeo

Comparison of two schemes for Laplace-domain 2D scalar wave equation

Jing-Bo Chen *, Shu-Hong Cao

Key Laboratory of Petroleum Resources Research, Institute of Geology and Geophysics, Chinese Academy of Sciences, P.O. Box 9825, Beijing 100029, China

ARTICLE INFO

Article history:
Received 4 December 2013
Accepted 14 April 2014
Available online 21 April 2014

Keywords:
Seismic modeling
Laplace domain
Average-derivative method
Finite-element method

ABSTRACT

Laplace-domain modeling plays an important role in Laplace-domain full waveform inversion. In order to provide efficient numerical schemes for Laplace-domain modeling, two 9-point schemes for Laplace-domain 2D scalar equation are compared in this paper. Compared to the finite-element 9-point scheme, the average-derivative optimal 9-point scheme reduces the number of grid points per pseudo-wavelength from 16 to 4 for equal directional sampling intervals. For unequal directional sampling intervals, the average-derivative optimal 9-point scheme reduces the number of grid points per pseudo-wavelength from 13 to 4. Numerical experiments demonstrate that the average-derivative optimal 9-point scheme is more accurate than the finite-element 9-point scheme for the same sampling intervals. By using smaller sampling intervals, the finite-element 9-point scheme can approach the accuracy of the average-derivative optimal 9-point scheme, but the corresponding computational cost and storage requirement are much higher.

1. Introduction

Using the zero frequency component of the damped wavefield, Laplace-domain full waveform inversion (FWI) can yield a smooth velocity model which can be used as a starting model for subsequent frequency-domain full waveform inversion (Shin and Cha, 2008). Because of its less sensitivity to the lack of low-frequency component, Laplace-domain FWI has been successfully applied to real data (Ha et al., 2012; Shin et al., 2010). Forward modeling in Laplace-domain is an essential part of Laplace-domain FWI. Therefore, it is important to make comparisons between different Laplace-domain schemes and provide efficient schemes for Laplace-domain FWI.

Laplace-domain schemes can be directly obtained from frequency-domain schemes. Frequency-domain schemes for 2D scalar wave equation include the classical 5-point scheme (Pratt and Worthington, 1990), the optimal 9-point scheme for equal directional sampling intervals (Jo et al., 1996; Operto et al., 2007), the average-derivative optimal scheme (Chen, 2012), and the directional-derivative method (Chen, 2013). However, the dispersion analysis of Laplace-domain schemes is different from that of frequency-domain schemes. Shin et al. (2002) developed a method to perform Laplace-domain numerical dispersion analysis by expressing Laplace-domain dispersion relation as the square root of the ratio of numerical eigenvalue to analytical eigenvalue. However, this dispersion relation depends on damping constant, velocity, and sampling interval as well as propagation angle. Therefore, it is difficult to draw a general conclusion and to optimize the scheme. Based on the skin depth in Laplace-domain acoustic wave equation (Um et al., 2012), Chen (2014) developed a Laplace-domain method of numerical dispersion analysis by defining a pseudo-wavelength as 2π times the skin depth. The dispersion relation can be expressed as a normalized attenuation propagation velocity which depends on the number of grid points per pseudo-wavelength as well as propagation angle.

In this paper, we use the method in Chen (2014) to make comparisons between two 9-point schemes for 2D Laplace-domain scalar wave equation. In the next section, we will present the Laplace-domain average-derivative optimal 9-point scheme and the finite-element 9-point scheme. This is followed by comparisons between the two schemes in terms of numerical dispersion analysis. Numerical examples are then presented to demonstrate the theoretical analysis.

2. Two Laplace-domain 9-point schemes

Consider the two-dimensional (2D) scalar wave equation in Laplace domain (Shin et al., 2002):

$$\frac{\partial^2 P}{\partial x^2}+\frac{\partial^2 P}{\partial z^2}-\frac{s^2}{v^2}P=0, \tag{1}$$

where P is the pressure wavefield, the real number s is the Laplace damping constant, and $v(x, z)$ is the velocity.

* Corresponding author.
E-mail address: chenjb@mail.iggcas.ac.cn (J.-B. Chen).

http://dx.doi.org/10.1016/j.jappgeo.2014.04.009
0926-9851/

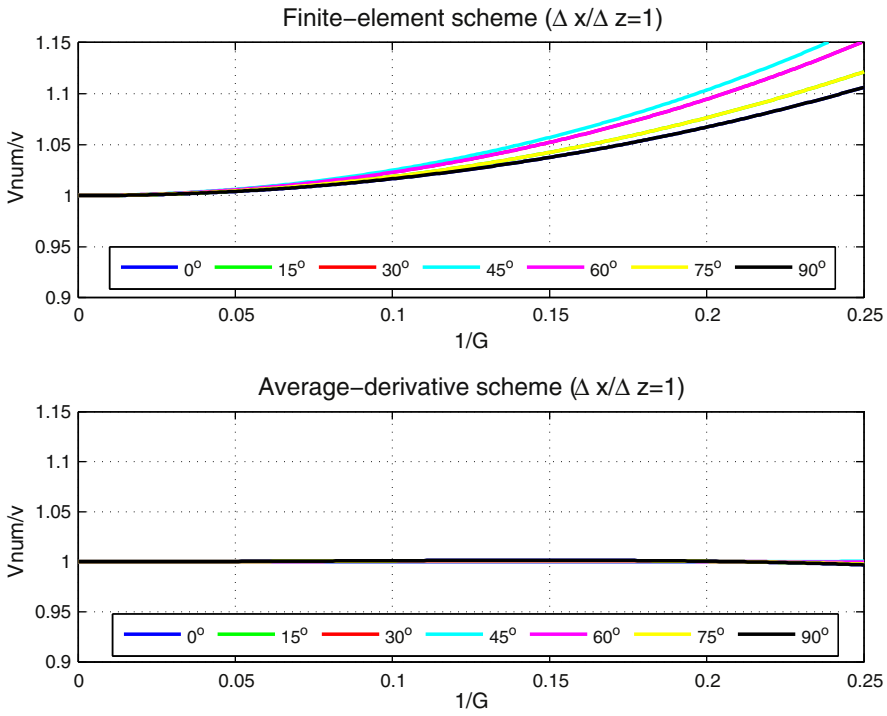

Fig. 1. Normalized numerical attenuation propagation velocity of the finite-element 9-point scheme (5) and the average-derivative optimal 9-point scheme (2) for different propagation angles for the case when $\frac{\Delta x}{\Delta z}=1$.

Based on the frequency-domain scheme developed in Chen (2012), one can obtain an average-derivative 9-point scheme for Eq. (1):

$$\begin{aligned}&\frac{\overline{P}_{m+1,n}-2\overline{P}_{m,\,n}+\overline{P}_{m-1,\,n}}{\Delta x^2}+\frac{\widetilde{P}_{m,\,n+1}-2\widetilde{P}_{m,\,n}+\widetilde{P}_{m,\,n-1}}{\Delta z^2}\\&-\frac{s^2}{v_{m,\,n}^2}\Big[cP_{m,\,n}+d\Big(P_{m+1,\,n}+P_{m-1,\,n}+P_{m,\,n+1}+P_{m,\,n-1}\Big)\\&+b\Big(P_{m+1,\,n+1}+P_{m-1,\,n+1}+P_{m+1,\,n-1}+P_{m-1,\,n-1}\Big)\Big]=0,\end{aligned}\tag{2}$$

where

$$\overline{P}_{m+j,n}=\frac{1-\alpha}{2}P_{m+j,n+1}+\alpha P_{m+j,n}+\frac{1-\alpha}{2}P_{m+j,n-1},\quad j=1,0,-1,\tag{3}$$

$$\widetilde{P}_{m,n+j}=\frac{1-\beta}{2}P_{m+1,n+j}+\beta P_{m,n+j}+\frac{1-\beta}{2}P_{m-1,n+j},\quad j=1,0,-1.\tag{4}$$

Here $P_{m,n}\approx P(m\Delta x,n\Delta z)$, $v_{m,n}\approx v(m\Delta x,n\Delta z)$, Δx and Δz are sampling intervals in x- and z-directions, respectively, α,β,c and d are weighted coefficients which should be optimized, and $b=\frac{1-c-4d}{4}$ (Chen, 2014).

Based on finite-element formulation, Shin et al. (2002) derived the following Laplace-domain finite-element 9-point scheme:

$$\begin{aligned}&\frac{1}{6}\frac{1}{\Delta x^2}\Big[P_{m+1,\,n-1}-2P_{m,\,n-1}+P_{m-1,\,n-1}\Big]\\&+\frac{2}{3}\frac{1}{\Delta x^2}\Big[P_{m+1,\,n}-2P_{m,\,n}+P_{m-1,\,n}\Big]\\&+\frac{1}{6}\frac{1}{\Delta x^2}\Big[P_{m+1,\,n+1}-2P_{m,\,n+1}+P_{m-1,\,n+1}\Big]\\&+\frac{1}{6}\frac{1}{\Delta z^2}\Big[P_{m-1,\,n+1}-2P_{m-1,\,n}+P_{m-1,\,n-1}\Big]\\&+\frac{2}{3}\frac{1}{\Delta z^2}\Big[P_{m,\,n+1}-2P_{m,\,n}+P_{m,\,n-1}\Big]\\&+\frac{1}{6}\frac{1}{\Delta z^2}\Big[P_{m+1,\,n+1}-2P_{m+1,\,n}+P_{m+1,\,n-1}\Big]-\frac{s^2}{v_{m,\,n}^2}P_{m,\,n}=0.\end{aligned}\tag{5}$$

Note that the scheme (5) is a special case of the scheme (2). If one takes $\alpha=\beta=\frac{2}{3}$, $c=1$, and $d=0$, then the scheme (2) becomes the scheme (5).

3. Comparison between two 9-point schemes

Consider an attenuating function in the following form

$$P(k,r)=P_0e^{-kr},\tag{6}$$

where $r=\sin(\theta)x+\cos(\theta)z$, P_0 is the amplitude at $r=0$, θ is the propagation angle, and k is the pseudo-wavenumber.

Substituting Eq. (6) into Eq. (2) and assuming a constant v, one obtains the discrete dispersion relation

$$\frac{V_{num}}{v}=\frac{G}{2\pi}\sqrt{\frac{A}{B}},\tag{7}$$

where

$$\begin{aligned}A=&\left[(1-\alpha)\cosh\left(\frac{2\pi\cos(\theta)}{RG}\right)+\alpha\right]\left[2\cosh\left(\frac{2\pi\sin(\theta)}{G}\right)-2\right]\\&+R^2\left[(1-\beta)\cosh\left(\frac{2\pi\sin(\theta)}{G}\right)+\beta\right]\left[2\cosh\left(\frac{2\pi\cos(\theta)}{RG}\right)-2\right],\\B=&c+2d\left[\cosh\left(\frac{2\pi\cos(\theta)}{RG}\right)+\cosh\left(\frac{2\pi\sin(\theta)}{G}\right)\right]\\&+4b\cosh\left(\frac{2\pi\cos(\theta)}{RG}\right)\cosh\left(\frac{2\pi\sin(\theta)}{G}\right),\end{aligned}$$

where $V_{num}=\frac{\omega}{k}$ is the numerical propagation velocity of attenuation, $G=\frac{2\pi}{k\Delta x}$ is the number of grid point per pseudo-wavelength, and $R=\frac{\Delta x}{\Delta z}$. Here, we only consider the case when $\Delta x\geq\Delta z$. The case when $\Delta x<\Delta z$ can be discussed similarly (Chen, 2014).

For the scheme (5), its discrete dispersion relation is a special case of Eq. (7) where $\alpha=\beta=\frac{2}{3}$, $c=1$, and $d=0$.

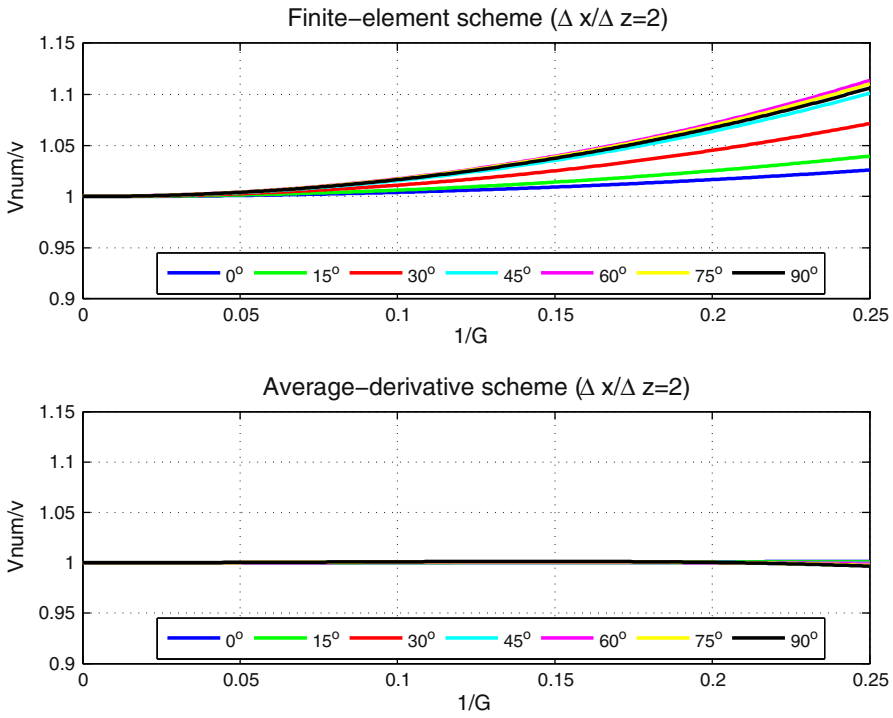

Fig. 2. Normalized numerical attenuation propagation velocity of the finite-element 9-point scheme (5) and the average-derivative optimal 9-point scheme (2) for different propagation angles for the case when $\frac{\Delta x}{\Delta z} = 2$.

Now we perform dispersion comparisons between the two 9-point schemes presented in the previous section. Fig. 1 shows normalized numerical attenuation propagation velocity of the finite-element 9-point scheme (5) and the average-derivative optimal 9-point scheme (2) for different propagation angles for the case when $\frac{\Delta x}{\Delta z} = 1$. For the finite-element 9-point scheme (5), the velocity errors increase with increasing $\frac{1}{G}$ for all propagation angles. At larger values of $\frac{1}{G}$, the errors become very large. Note that the normalized numerical attenuation propagation velocity for propagation angle θ is equal to that for propagation angle $90°-\theta$. This is consistent with Eq. (7). On the other hand, for the average-derivative optimal 9-point scheme (2), the velocity errors remain small for all values of $\frac{1}{G}$ and θ. In this case, the optimal coefficients for the scheme (2) are $\alpha = 0.863852$, $\beta = 0.863852$, $c = 0.693994$, and $d = 0.076501$ (Chen, 2014). From Fig. 1, one can draw a conclusion that

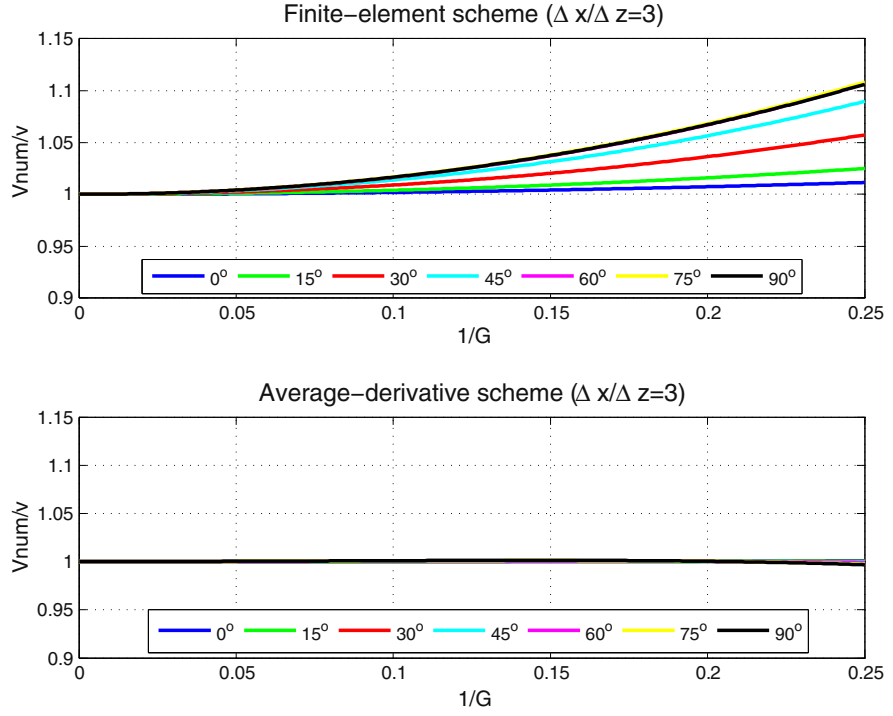

Fig. 3. Normalized numerical attenuation propagation velocity of the finite-element 9-point scheme (5) and the average-derivative optimal 9-point scheme (2) for different propagation angles for the case when $\frac{\Delta x}{\Delta z} = 3$.

within the relative error of 1%, the finite-element 9-point scheme (5) requires 16 grid points per pseudo-wavelength, while the average-derivative optimal 9-point scheme (2) requires 4 grid points per pseudo-wavelength for equal directional sampling intervals.

Figs. 2 and 3 show normalized numerical attenuation propagation velocity of the finite-element 9-point scheme (5) and the average-derivative optimal 9-point scheme (2) for different propagation angles for the cases when $\frac{\Delta x}{\Delta z}=2$, and $\frac{\Delta x}{\Delta z}=3$, respectively. In these two cases, the normalized numerical attenuation propagation velocity for propagation angle θ is no longer equal to that for propagation angle 90°−θ. This is also consistent with Eq. (7). As for velocity errors, the conclusions are similar to that of the case when $\frac{\Delta x}{\Delta z}=1$. The optimal coefficients for the scheme (2) are $\alpha=0.828891$, $\beta=0.866232$, $c=0.693025$, and $d=0.076743$ for $\frac{\Delta x}{\Delta z}=2$, and $\alpha=0.834753$, $\beta=858629$, $c=0.693395$, and $d=0.076651$ for $\frac{\Delta x}{\Delta z}=3$, respectively (Chen, 2014). From Figs. 2 and 3, one can draw a conclusion that within the relative error of 1%, the finite-element 9-point scheme (5) requires 13 grid points per pseudo-wavelength, while the average-derivative optimal 9-point scheme (2) requires 4 grid points per pseudo-wavelength for unequal directional sampling intervals.

For a heterogeneous media, the grid size is usually determined by using the minimum velocity. Another choice is to use the average velocity (Shin et al., 2002).

4. Numerical examples

First, we consider a homogeneous velocity model with a velocity of 2000 m/s. Horizontal and vertical distances are both 10 km (Fig. 4a). The Laplace damping constant s is taken to be 10π. Accordingly, the pseudo-wavelength is $\lambda = 2000/(10\pi/2\pi)\ \text{m} = 400$ m. According to the criterion of 4 grid points per smallest pseudo-wavelength, horizontal sampling interval is determined by $\Delta x = 400/4\ \text{m} = 100$ m. Vertical sampling interval is taken as $\Delta z = \Delta x/2 = 50$ m. Horizontal and vertical samplings are $nx = 101$ and $nz = 201$, respectively. A Ricker wavelet is placed at the center of the model as a source, and a receiver array is placed at a depth of 2.5 km. For the analytical solution, the following formula is used (Alford et al., 1974):

$$P(x,z,s) = i\pi H_0^{(2)}\left(\frac{-is}{v}d\right)F(s), \tag{8}$$

where i is the imaginary unit, $H_0^{(2)}$ is the second Hankel function of order zero, $F(s)$ is the Laplace transform of the Ricker wavelet, and $d=\sqrt{(x-x_0)^2+(z-z_0)^2}$. Here (x_0, z_0) is the source position.

Fig. 4b shows the Laplace-domain seismograms computed with the analytical formula (8), the finite-element 9-point scheme (5) and the average-derivative optimal 9-point scheme (2). The simulation result with the average-derivative optimal 9-point scheme (2) is in good agreement with the analytical result. The result with the finite-element 9-point scheme (5) exhibits errors which become larger as the offset increases.

Second, we consider a heterogeneous model. Fig. 5a shows a salt model which is a two-dimensional section of the SEG/EAGE salt

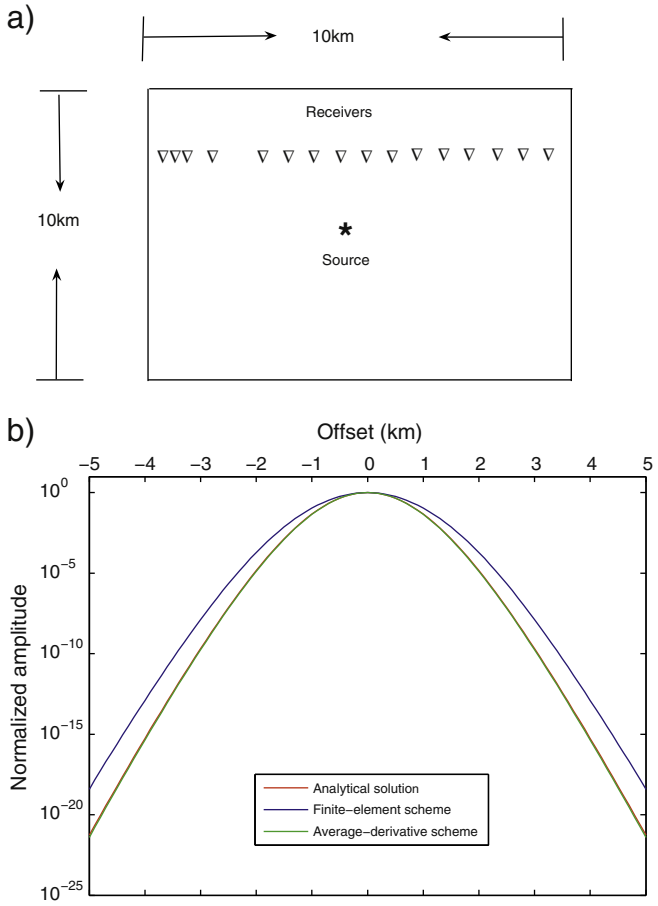

Fig. 4. (a) Schematic of the homogenous model. (b) Laplace-domain seismograms computed with the analytical formula (8), the finite-element 9-point scheme (5) and the average-derivative optimal 9-point scheme (2).

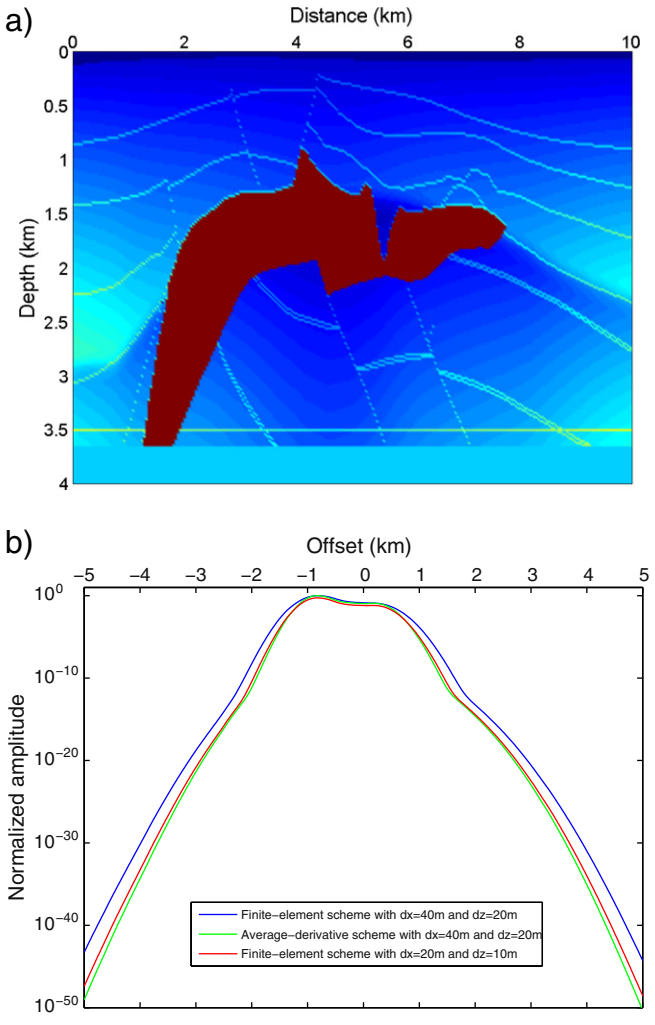

Fig. 5. (a) The salt model. (b) Laplace-domain seismograms computed with the finite-element 9-point scheme (5) with $\Delta x = 40$ m and $\Delta z = 20$ m, the average-derivative optimal 9-point scheme (2) with $\Delta x = 40$ m and $\Delta z = 20$ m and the finite-element 9-point scheme (5) with $\Delta x = 20$ m and $\Delta z = 10$ m.

model. The sampling intervals are $\Delta x = 40$ m and $\Delta z = 20$ m. Horizontal and vertical samplings are $nx = 251$ and $nz = 201$, respectively. A Ricker wavelet is placed at ($x = 5$ km, $z = 2$ km) as a source, and the receivers are set at the depth of 20 m with a spacing of 40 m. The Laplace damping constant s is taken to be 10π. Fig. 5b shows the Laplace-domain seismograms computed with the finite-element 9-point scheme (5) and the average-derivative optimal 9-point scheme (2). Since the analytical solution is not available in this case, we also show the result computed with the finite-element 9-point scheme (5) with smaller Δx and Δz for comparison. One can see that the result of the finite-element 9-point scheme (5) with $\Delta x = 20$ m and $\Delta z = 10$ m is closer to the result of the average-derivative optimal 9-point scheme (2) with $\Delta x = 40$ m and $\Delta z = 20$ m. This demonstrates the greater accuracy of the average-derivative optimal 9-point scheme (2) for this salt model. It should be noted that the computational cost and storage requirement are much higher when using smaller spacings. In terms of this salt model, when using smaller spacings, the storage requirement is 8 times higher and the computational cost is 5 times higher.

5. Conclusions

Based on dispersion analysis and numerical experiments, an average-derivative optimal 9-point scheme and a finite-element 9-point scheme are compared. The finite-element 9-point scheme requires 16 grid points per pseudo-wavelength for equal directional sampling intervals and 13 grid points per pseudo-wavelength for unequal directional sampling intervals. In contrast, the average-derivative optimal 9-point scheme requires 4 grid points per pseudo-wavelength for both equal and unequal directional sampling intervals. The numerical example for a homogeneous model demonstrates that the average-derivative optimal 9-point scheme is more accurate than the finite-element 9-point scheme when using the same sampling intervals. The numerical example for the salt model shows that the finite-element 9-point scheme can approach the accuracy of the average-derivative optimal 9-point scheme by using smaller sampling intervals at much higher cost of CPU time and storage requirement.

Acknowledgments

This work is supported by National Natural Science Foundation of China under grant nos. 41274139 and 40974074.

References

Alford, R.M., Kelly, K.R., Boore, D.M., 1974. Accuracy of finite-difference modeling of the acoustic wave equation. Geophysics 39, 834–842.
Chen, J.-B., 2012. An average-derivative optimal scheme for frequency-domain scalar wave equation. Geophysics 77 (6), T201–T210.
Chen, J.-B., 2013. A generalized optimal 9-point scheme for frequency-domain scalar wave equation. J. Appl. Geophys. 92, 1–7.
Chen, J.-B., 2014. Dispersion analysis of an average-derivative optimal scheme for Laplace-domain scalar wave equation. Geophysics 79 (2), T37–T42.
Ha, W., Chung, W., Park, E., Shin, C., 2012. 2-D acoustic Laplace-domain waveform inversion of marine field data. Geophys. J. Int. 190, 421–428.
Jo, C.-H., Shin, C., Suh, J.H., 1996. An optimal 9-point, finite-difference, frequency-space, 2-D scalar wave extrapolator. Geophysics 61, 529–537.
Operto, S., Virieux, J., Amestoy, P., L'Excellent, J.-Y., Giraud, L., Ali, H.B.H., 2007. 3D finite-difference frequency-domain modeling of visco-acoustic wave propagation using a massively parallel direct solver: a feasibility study. Geophysics 72 (5), SM195–SM211.
Pratt, R.G., Worthington, M.H., 1990. Inverse theory applied to multi-source cross-hole tomography, part I: scalar wave-equation method. Geophys. Prospect. 38, 287–310.
Shin, C., Cha, Y.H., 2008. Waveform inversion in the Laplace domain. Geophys. J. Int. 173, 922–931.
Shin, C., Min, D.J., Marfurt, K.J., Lim, H.Y., Yang, D., Cha, Y.H., Ko, S., Yoon, K., Ha, T., Hong, S., 2002. Traveltime and amplitude calculations using the damped wave solution. Geophysics 67, 1637–1647.
Shin, C., Cha, Y.H., Park, K.P., 2010. Sequentially ordered single-frequency 2-D acoustic waveform inversion in the Laplace–Fourier domain. Geophys. J. Int. 181, 935–950.
Um, E.S., Commer, M., Newman, G.A., 2012. Iterative finite-difference solution analysis of acoustic wave equation in the Laplace–Fourier domain. Geophysics 77 (2), T29–T36.